THE OPTIMAL CONTROL SOLVER

BOCOP - A collection of examples

Frédéric Bonnans, Pierre Martinon
D. Giorgi, V. Grélard, B. Heymann, J. Liu, S. Maindrault, O. Tissot

October 2, 2017

Contents

1 Overview

The Bocop project aims to develop an open-source toolbox for solving optimal control problems, with collaborations involving industrial and academic partners. Optimal control (optimization of dynamical systems governed by differential equations) has numerous applications in the fields of transportation, energy, process optimization, and biology. It began in 2010 in the framework of the Inria-Saclay initiative for an open source optimal control toolbox, and is supported by the team Commands.

The original BOCOP package implements a local optimization method. The optimal control problem is approximated by a finite dimensional optimization problem (NLP) using a time discretization (the direct transcription approach). The NLP problem is solved by the well known software IPOPT, using sparse exact derivatives computed by ADOL-C.

The second package BOCOPHJB implements a global optimization method. Similarly to the Dynamic Programming approach, the optimal control problem is solved in two steps. First we solve the Hamilton-Jacobi-Bellman equation satisfied by the value function of the problem. Then we simulate the optimal trajectory from any chosen initial condition. The computational effort is essentially taken by the first step, whose result, the value function, can be stored for subsequent trajectory simulations.

Please visit the website for the latest news and updates.

Website: http://bocop.org
Contact: Pierre Martinon (`pierre.martinon@inria.fr`).

In this document we present a collection of classical optimal control problems which have been implemented and solved with Bocop. We recall the main features of the problems and of their solutions, and describe the numerical results obtained. The presented numerical tests generally use 100 time steps or so, with initialization of the control and state variables by simple constant values. The solution is usually computed in a few seconds.

Users are encouraged to experiment with the data in these problems in order to get acquainted with the use of Bocop. It is interesting to observe how the convergence is affected by changes in the initialisation of the control and state, the number of time steps, or the discretization scheme. A further step might be to make changes in the dynamics or cost function.

We hope that providing these documented examples will help users to write and solve their own applications with Bocop. The following problems are sorted in four general categories: integrator systems, process control, mechanical systems and aerospace, and PDE control of parabolic equations.

2 Integrator systems

2.1 Generic form

We consider *integrator systems* of the form

$$x^{(k)}(t) = u(t), \quad t \in [0, T], \tag{1}$$

for $k = 1$ to 3. The state variables are therefore $y_1 = x$, and for $k > 1$, $y_2 = \dot{x}, \ldots, y_k = x^{(k-1)}$. The cost function is $\int_0^T \ell(t, u(t), y(t))dt$, with

$$\ell(t, u(t), y(t)) := \alpha x(t) + \beta_1 x^2(t) + \beta_2 \dot{x}^2(t) + \gamma u(t) + \delta u^2(t). \tag{2}$$

Setting the constants $\alpha, \ldots, \delta$ allows for a wide variety of cost functions (note that of course $\beta_2 = 0$ when $k = 1$). We add the control and state constraints for all t

$$u(t) \in [-1, 1]; \quad y(t) \geq a. \tag{3}$$

2.2 First-order system

While these examples are very simple, they nevertheless show some typical behavior that will be extended later to higher order systems. Consider first the problem

$$\begin{cases} Min \displaystyle\int_0^T x^2(t) + \gamma u(t) + \delta u^2(t) \quad dt \\ \dot{x}(t) = u(t), \quad t \in [0, T], \quad x(0) = x^0. \end{cases} \tag{4}$$

If $(\gamma, \delta) = (1, 0)$, $x(0) = 1$, and $T > 1$, then the solution is $u(t) = -1$ for $t \in [0, 1]$, and $u(t) = 0$ for $t > 1$. In particular, the control is discontinuous but piecewise continuous. If we change δ to a small positive value, say 0.1, we see that the control is continuous, althought it varies sharply when the time comes close to 1.

The user may experiment what happens when the state constraint threshold a is positive: again the control is discontinuous when $\delta = 0$, and continuous when $\delta > 0$.

We next discuss the optimal control of two second order integrator systems.

2.3 Fuller problem [Bocop] [BocopHJB]

Here is a very classical example of a chattering phenomenon describeb by Fuller [14]:

$$Min \int_0^T x^2(t)dt; \quad \ddot{x}(t) = u(t) \in [-1, 1]. \tag{5}$$

The solution is, for large enough T, bang-bang (i.e., with values alternately ± 1), the switching times geometrically converging to a value $\tau > 0$, and then the (trivial) *singular arc* $x = 0$ and $u = 0$. These switches are not easy to reproduce numerically.

Simulations with BOCOP and BOCOPHJB are shown on Figs 1-2. We take here $T = 3.5$, $x(0) = 0, \dot{x}(0) = 1$, $x(T) = \dot{x}(T) = 0$ and $u(t) \in [-1, 1]$. We observe that the HJB method does not find the correct chattering structure for the control. The state trajectory, however, is close to the optimal one, with an objective value of 0.2789 versus 0.2731. On this problem, applying Pontryagin's Principle indicates that the optimal control is either bang (-1 or 1) or singular (0). Therefore we can use only these 3 values to discretize the control, which gives a similar solution with faster computations.

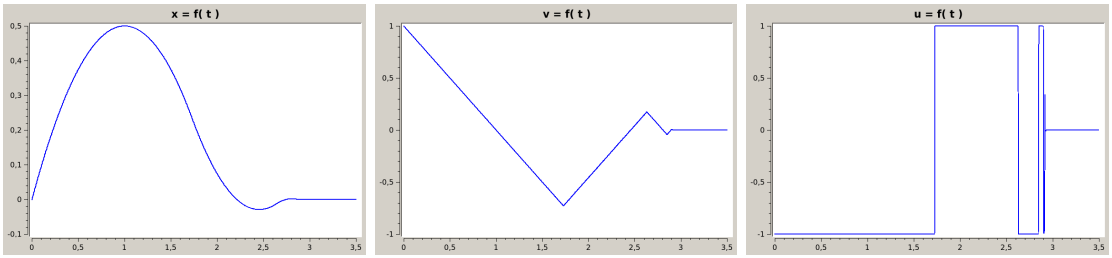

Figure 1: **fuller:** state x, v and chattering control u

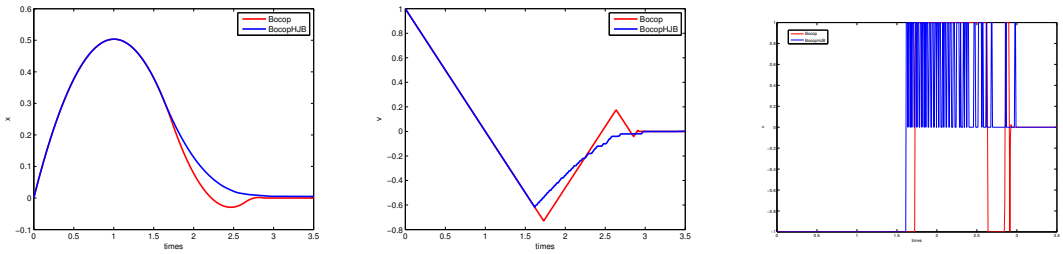

Figure 2: **fuller (BocopHJB):** state x, v and control u

2.4 Relaxed oscillations problem [BocopHJB]

We consider the optimal control problem

$$\begin{array}{l} \min \int_0^1 y^2 - u^2 \\ \dot{y} = u \\ u \in [-1, 1] \end{array}$$

The Hamiltonian is $H = y^2 - u^2 + up$. A minimizing control u^* is either -1 or 1. The intuition is that the control has to oscillate very quickly between -1 and 1 to obtain the optimal value. The infimum is -1, as attained for instance with the sequence of controls $u_n(t) = 1$ if $t \in [\frac{2k}{2^n}, \frac{2k+1}{2^n}]$, -1 otherwise.

Consider that the control is randomized at any time, with probability α for $u = 1$. We can formulate the relaxed problem

$$\begin{array}{l} \min \int_0^1 y^2 - 1 \\ \dot{y} = \mathbb{E}(u) = \alpha 1 + (1-\alpha)(-1) = 2\alpha - 1 \\ \alpha \in [0,1] \end{array}$$

The optimal solution for the relaxed problem is given by $\alpha = 0.5$. Therefore when solving the original problem with the dynamic programming principle, we expect the simulated trajectory to present a sequence of very fast oscillations.

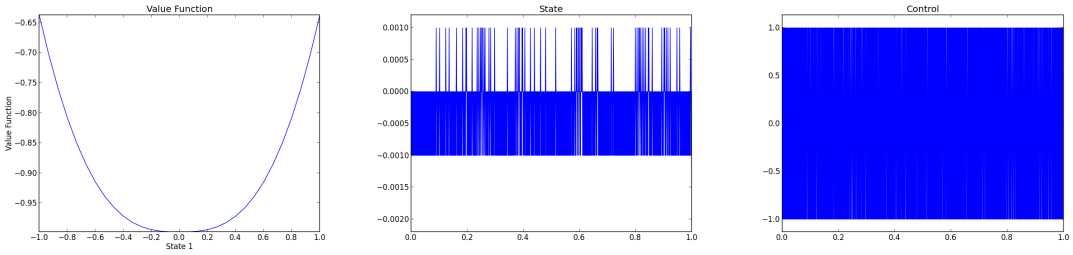

Figure 3: **relaxed (BocopHJB):** value function (left) and optimal trajectory (state, control). The trajectory exhibits the oscillations predicted by the relaxed problem.

2.5 Second order singular regulator [Bocop] [BocopHJB]

We consider a second order singular regulator problem, see Aly [2], or [3]:

$$Min \int_0^T x^2(t) + \dot{x}^2(t) \quad dt; \quad \ddot{x}(t) = u(t) \in [-1, 1]. \tag{6}$$

The difference with Fuller's problem is that the cost function includes a penalization of the "speed" $\dot{x}(t)$. Taking for instance $T = 5$, $x(0) = 0, \dot{x}(0) = 1$, we observe in figure 4-5 the occurrence of a singular arc. The optimal control has a structure *(Bang(-1) - Singular)*.

State constraint. Now we add the pure state constraint $\dot{x}(t) \geq -0.25$. This changes the structure of the optimal control from *(Bang(-1) - Singular)* to *(Bang(-1) - Constrained(0) - Singular)*, cf fig. 6.

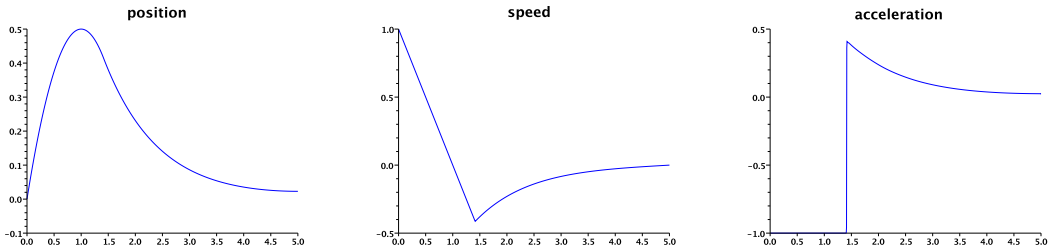

Figure 4: **regulator:** state and control (bang-singular structure).

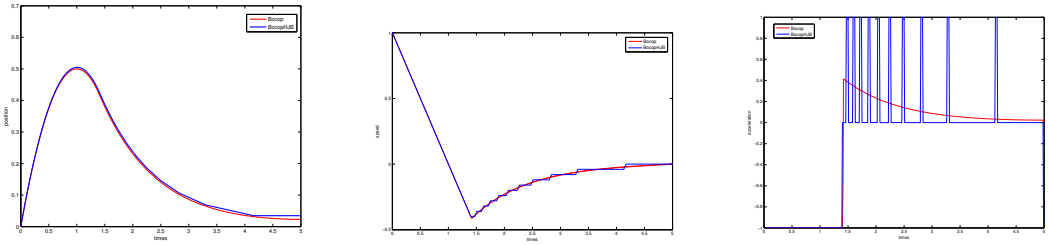

Figure 5: **regulator (BocopHJB):** state and control. The singular arc is correctly captured on the state variables, even though the singular control is not.

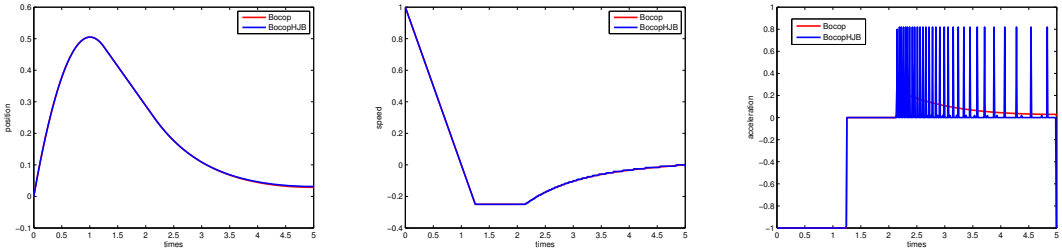

Figure 6: State constraint. The control structure is now (Bang(-1) - Constrained(0) - Singular). Once again the HJB method finds the correct singular arc with respect to the state variables, but not the singular control.

2.6 Third order state constraints [Bocop]

Robbins [33] considered the following family of problems:

$$Min \frac{1}{2}\int_0^T \alpha y(t) + \frac{1}{2}u(t)^2 \quad dt; \quad y^{(3)}(t) = u(t); \;\; y(t) \geq 0,$$

and proved that, for appropriate initial conditions, the exact solution has infinitely many isolated contact points, such that the length of unconstrained arcs decreases geometrically. The isolated contact points have an accumulation point, followed by the trivial singular arc $u = 0$, $y = 0$. Detailed computations can be found in [21]. It is not easy to reproduce numerically this behaviour, since the unconstrained arcs rapidly become too small to be

captured by a given time discretization. We display in Figure 7 the value of the first state component and of the control, computed with Bocop. We take here $\alpha = 3$, $T = 10$, $y(0) = 1$, $\dot{y}(0) = -2$, $\ddot{y}(0) = 0$.

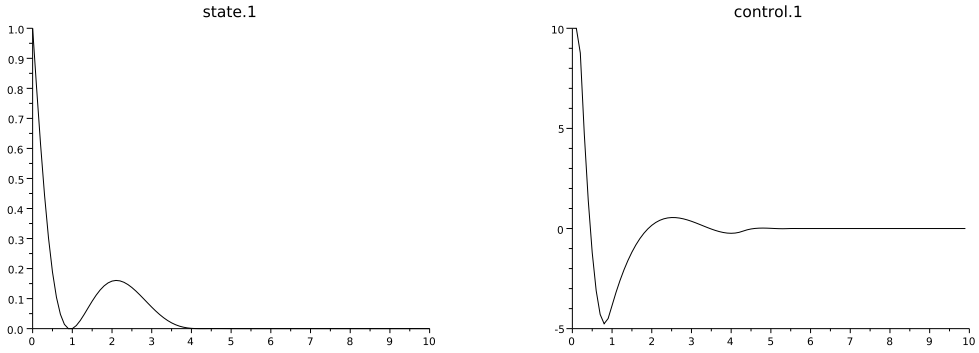

Figure 7: **robbins:** first order state constraint and control.

It seems that no "generic" (stable with respect to a perturbation) example of a third order state constraint with a regular entry/exit point for a singular arc is known. It is conjectured that no such point exists. Jacobson et al. [25] considered the following example:

$$Min \frac{1}{2} \int_0^T u(t)^2 \, dt; \;\; y^{(3)}(t) = u(t); \;\; y(t) \leq y_{max}.$$

with initial condition for which there is no boundary arc, and one or two touch points.

Fourth order state constraints

No example with a nontrivial boundary arc is known, and it is conjectured that this does not occur. Let us mention the example studied by Jacobson et al. [25]:

$$Min \frac{1}{2} \int_0^T u(t)^2 \, dt; \;\; y^{(4)}(t) = u(t); \;\; |y(t)| \leq y_{max}.$$

3 Process control

3.1 Bio-reactor converting micro-algae to methane [Bocop]

Coupling microalgae culture and anaerobic digestion is a promising process to convert solar energy into methane. In [6, 5] we consider a dual-tank reactor: a first one in which microalgae are cultivated and a second one where the microalgae are converted into biogas. Our first aim is to find an optimal feeding strategy in order to maximize the production of biogas in the second reactor during one day.

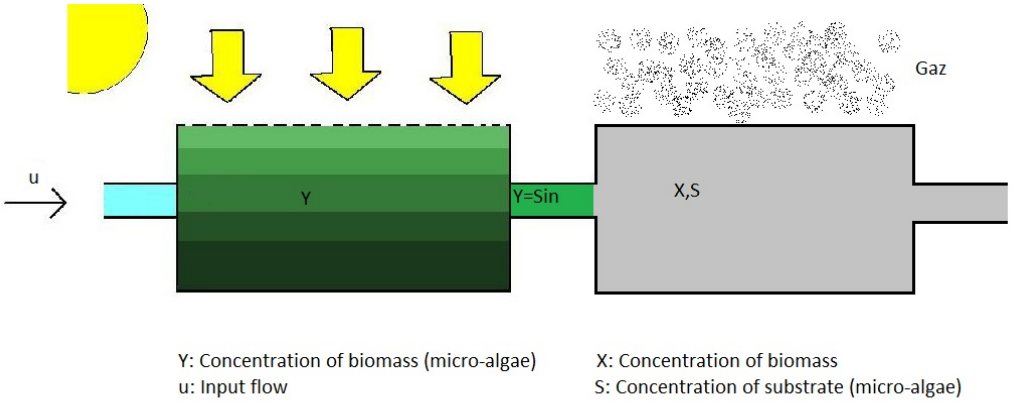

Figure 8: A dual tank bioreactor for converting microalgae into methane

The dual-tank bioreactor can be modeled as a 3-dimensional dynamical system. The state variables are the concentration of micro-algae y, biomass x and substrate s. The control variable is the input flow u throughout the whole reactor. The dynamics are

$$(*) \begin{cases} \frac{dy}{dt} = \frac{\mu(t)y}{1+y} - ry - uy \\ \frac{ds}{dt} = -\mu_2(s)x + u\beta(\gamma y - s) \\ \frac{dx}{dt} = [\mu_2(s) - u\beta]\, x \end{cases}$$

where μ is the light model, $\mu_2(s) = \mu_2^m \frac{s}{K_s+s}$ the growth function in reactor 2 (Monod), and β the volume ratio between the two tanks

The objective is to maximize the methane production over time, starting from initial concentrations free in a certain domain. We can add some optional periodicity conditions on the concentrations. The optimal control problem is written as

$$(OCP) \begin{cases} Max \frac{1}{\beta+c} \int_0^{t_f} \mu_2(s(t))x(t)dt \\ \frac{d}{dt}(y,s,x) = f(t,y,s,x,u)\ (*) \\ u \in [0,1] \\ (y(0),s(0),x(0)) \in Z_0 \\ (y(t_t),s(t_f),x(t_f)) = (y(0),s(0),x(0)) \quad (optional) \end{cases}$$

The optimal solution for a periodic optimization over 1 day is shown on Fig.9. Algae concentration increases during the first half of period ie day, then decreases at night.

Biomass concentration in the second tank is almost constant. Here the control structure is **0 - Singular - 0**, which is consistent with the Hamiltonian being linear in the control. The arcs $u = s = 0$ at the beginning and ending of the time frame are actually due to a limit in design, namely $\beta = 1$.

Generally speaking, simulations over a larger time period indicate that the optimal long-term strategy consists in three phases, see fig.10. First we observe an initial phase of growth, starting from the initial conditions to reach some optimal concentrations levels. Then for almost the whole time interval we see a sequence of identical, optimal 1-day periodic cycles. Finally there is a wash-out phenomenon at the end of the time frame, which is more a perturbation.

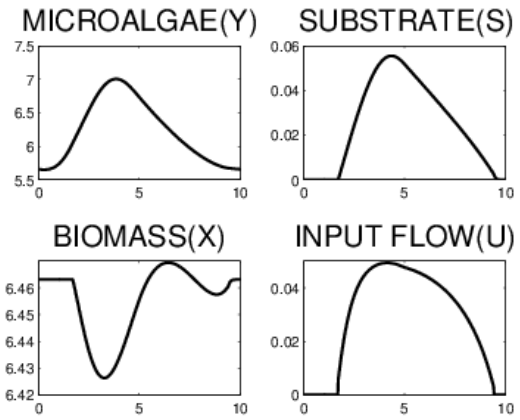

Figure 9: **bioreactor:** optimal 1-day periodic cycle

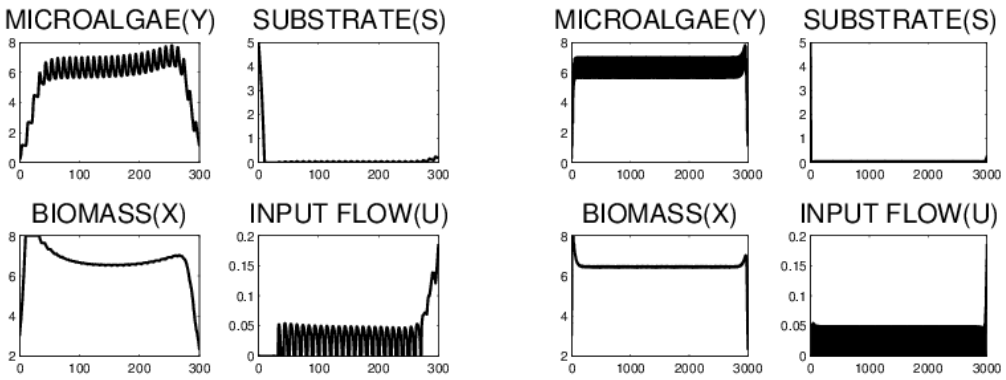

Figure 10: **bioreactor:** optimization over 30 and 300 days.

Attraction property

We also illustrate an attraction property of the dynamical system, established in [5]. We now set the control as the optimal solution from the 1-day periodic problem, and simulate the evolution of the system from different initial conditions. Simulations confirm this fixed

sequence of controls drives the system to an optimal mode, after which the trajectory becomes periodic, see fig.11. We can check that these periodic 1-day cycles are identical to the ones obtained when performing the full optimization with free control, cf fig.12.

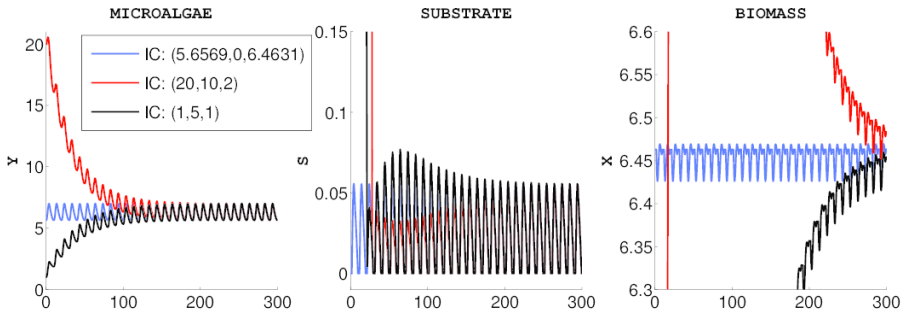

Figure 11: Attraction property (fixed periodic control, different initial conditions).

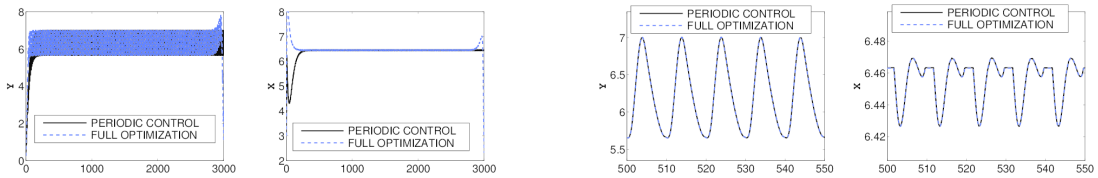

Figure 12: Fixed periodic control vs full optimization (with zoom).

Optimal tank volume ratio

Finally, we check this by solving the same problem while also optimizing the volume ratio β. It turns out the optimal ratio β^* depends on the optimization horizon, with an asymptotic value corresponding to the periodic 1-day optimization.

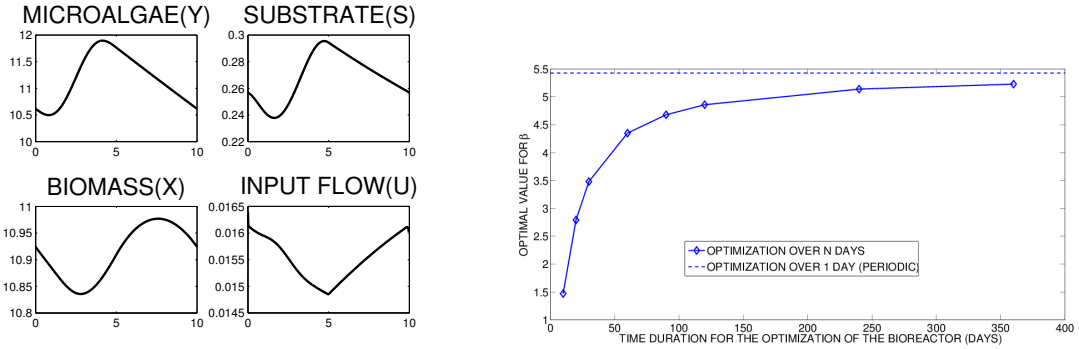

Figure 13: Optimizing the tank volume ratio β.

3.2 Jackson problem (parameter identification) [Bocop]

Consider the model in Jackson [24], also discussed in Biegler [7], of chemical reactions

$$A \overset{1}{\rightleftharpoons} B \overset{2}{\rightharpoonup} C$$

The first reaction is reversible, converting A to B and vice-versa, and the second one is one-sided, converting B to C. Here the control $u(t) \in [0, 1]$ is the fraction of catalyst which sets the balance between the reactions 1 and 2, and we want to maximize the production of C. The initial feed is assumed to consist of pure substance A. Noting a, b, c the mole fractions of A, B, C and k_1, k_2, k_3 the velocity constants of chemical reactions, the optimal control problem is written as

$$(OCP) \begin{cases} Max\ c(T) \\ \dot{a}(t) = -u(t)\,(k_1 a(t) - k_2 b(t)) \\ \dot{b}(t) = u(t)\,(k_1 a(t) - k_2 b(t)) - (1 - u(t)) k_3 b(t) \\ \dot{c}(t) = (1 - u(t)) k_3 b(t) \\ u(t) \in [0, 1] \\ a(0) = 1, b(0) = c(0) = 0 \end{cases}$$

Remark: note that since $a(t) + b(t) + c(t)$ is an invariant, we could eliminate one of the state variables.

The Hamiltonian being linear in the control, we expect a solution whose optimal control is a sequence of bang and/or singular arcs. We show on figure 14 the solution obtained for $k_1 = k_3 = 1, k_2 = 10$, and $T = 4$. In this case the control has one singular arc, with a **bang (1) - singular - bang(0)** structure.

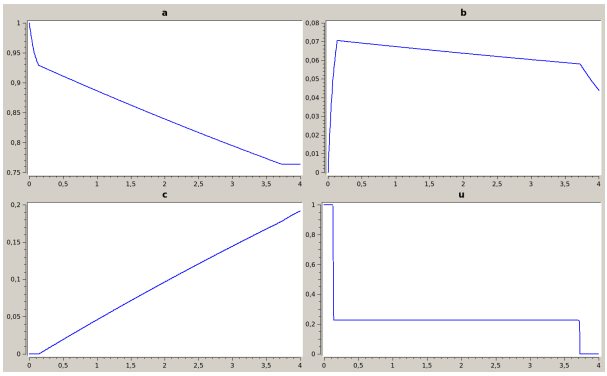

Figure 14: **jackson_basic:** concentrations a, b, c and control u.

Parameter identification with fixed control

Now we consider the velocity constants k_1, k_2 and k_3 as unknown parameters. We want to identify these parameters based on some observations of the concentrations $a(t)$, $b(t)$ and $c(t)$ from an experiment with a known control. Here we will replace the experiment with a simulation, taking for instance the constant control $u = 0.5$. For this simulation

we set the parameters to the values $k_1 = k_3 = 1, k_2 = 10$. We take some sample values from the simulation and add some small noise to reflect the errors in measurements, see fig.15. In this case we made the assumption that a, b and c were measured at different time steps, hence the use of weights equal to 0 or 1 in the observation file. Then we perform the identification on the k_i, using theses values as observation data, with the least square method featured in Bocop. The results of the identification are very close to the original values (Table 1).

```
# Data file for parameter identification
# taken from jackson solution with u= 0.5

# Time          Observations            Weights
0.4,    0.9144, 0.0753, 0,      1,      1,      0
0.8,    0.8928, 0.0810, 0,      1,      1,      0
1.2,    0,      0,      0.0424, 0,      0,      1
1.6,    0.8627, 0.0791, 0,      1,      1,      0
2,      0,      0,      0.0739, 0,      0,      1
2.4,    0.8342, 0.0764, 0,      1,      1,      0
3.2,    0.8067, 0.0739, 0,      1,      1,      0
4,      0.7799, 0.0715, 0.1488, 1,      1,      1
```

Figure 15: Comma-separated observation data

Parameter	k_1	k_2	k_3
Original value	1	10	1
Identified value	0.997614	9.97377	1.00095

Table 1: Parameter identification results

Problem variants

- jackson_id: basic parameter identification problem. Single observation file with 0 weights for missing values.
- jackson_id_2: Two separate observation files, one for a, b and the other for c. Observation times are specific to each file.
- jackson_id_3: Two separate data files again. Identification method is Manual, used to reproduce the least square criterion as an illustration.

4 Medical applications

4.1 Contrast in Magnetic Resonance Imaging (MRI) [Bocop]

A medical MRI device

Magnetic Resonance Imaging (MRI) is a medical imagery technique that does not expose the body to ionizing radiation such as X-ray. Instead, it relies on a strong magnetic field to excite atoms in the tissues, more specifically hydrogen atoms present in water (water accounts for 70% of the human body mass). Measuring the rate at which the atoms go back to their equilibrium state allows to reconstruct the spatial distribution of water, and by extension to differentiate tissue types.

Finding the magnetic field that maximizes the contrast between two types of tissue can be written as an optimal control problem, studied for instance in [9, 10]. The magnetization vector $q = (x, y, z) \in B(0, 1)$ for each 1/2 spin particle follows the Bloch equation

$$\begin{aligned} \dot{x} &= -\Gamma x + u_2 z \\ \dot{y} &= -\Gamma y - u_1 z \\ \dot{z} &= \gamma(1 - z) + u_1 y - u_2 x \end{aligned}$$

with u the magnetic field (control) and γ, Γ relaxation parameters depending on the tissue. In the simplified, two-dimensional mono-input case, we get

$$\begin{aligned} \dot{y} &= -\Gamma y - u_1 z \\ \dot{z} &= \gamma(1 - z) + u_1 y \end{aligned}$$

Considering two different particles with spins q_1, q_2, the contrast is linked to $|\|q_1\| - \|q_2\||$ at the end of the excitation phase. The classical "contrast by saturation" method consists in bringing one spin to the origin ("saturation") and the other as far as possible. Assuming both spins start from the equilibrium point at the north pole, the optimal control problem is

$$(OCP) \begin{cases} Max\ |q_2(t_f)| \\ \dot{q} = f(q, u) \\ |u(\cdot)| \leq 1 \\ q_1(0) = q_2(0) = (0, 1) \\ q_1(t_f) = 0 \end{cases}$$

with the final time set to a multiple of the minimum time T_{min} for the saturation of q_1, ie $t_f = \lambda T_{min}, \alpha \geq 1$. The Hamiltonian is linear in the control, and it can be shown ([12]) that the optimal control is a sequence of Bang and Singular arcs, noted nBS (ie 2BS denotes a bang-singular-bang-singular structure).

We illustrate this problem on the (cerebro-spinal fluid,water) case, see fig.16 ($\tau = t/t_f$ is the normalized time), with an example of a 2BS structure. A comprehensive study using indirect shooting and differential continuation methods (HAMPATH,[12]) indicates the existence of numerous families of local solutions with different structures, and shows that the optimal structure depends on the final time, as illustrated on fig.17.

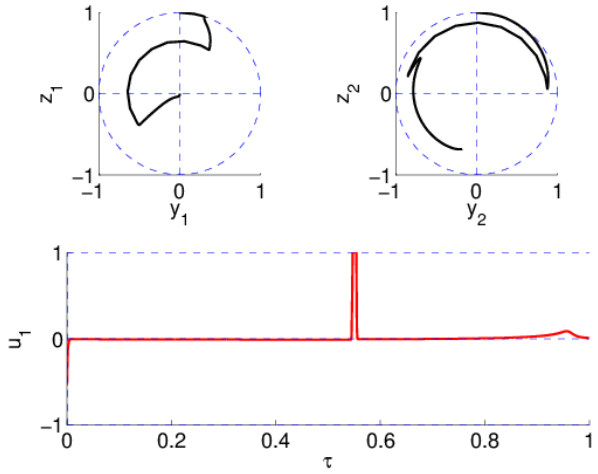

Figure 16: **contrast:** (cerebro-spinal fluid,water) case.

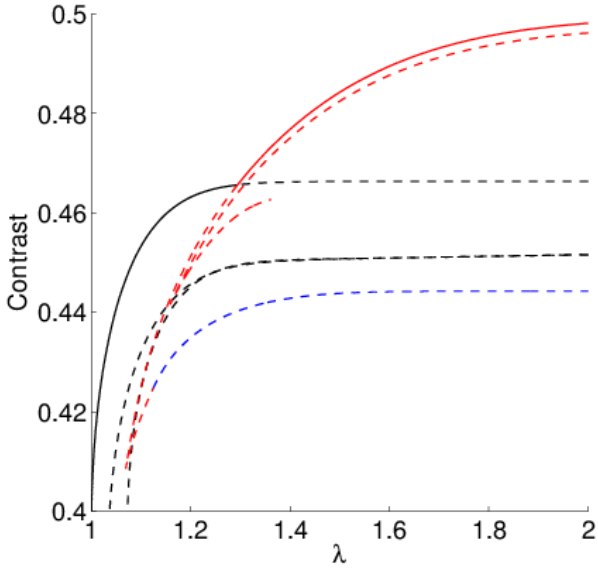

Figure 17: **contrast:** branches of local solutions (1BS: black, 2BS: blue, 3BS: red)

4.2 Control of leukemic cell population (delay) [Bocop]

We study the optimal control of leukemic cell population presented in [13], namely the optimal use of a combination of cytostatic and cytotoxic drugs in order to reduce the total cancerous cells. The model from [1, 28] considers two sub-populations of leukemic cells: the inactive resting cells, and the proliferating cells. Resting cells go into the proliferating phase at constant rate β. Proliferating cells either die by apoptosis with rate γ or divide during mitosis into two daughter cells. Mitosis has a duration of 2τ and the daughter cells start in the resting phase. We introduce the age variable a for the time spent in the proliferating phase, and note $R(t)$ the resting population and $p(a,t)$ the proliferating population. We consider two drugs: a cytotoxic that induces a death rate $u(t)$ in the second half of the proliferating phase, and a cytostatic v that results in a fraction $k(t)$ of inhibited resting cells that are blocked from entering the proliferating phase. This age-structured model is represented on Fig. 18.

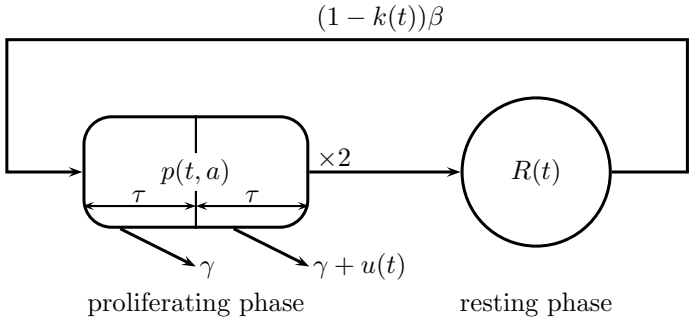

Figure 18: Age-structured model

The system follows the dynamics

$$\begin{aligned}
&\frac{dR}{dt}(t) = -(1-k(t))\beta R(t) + 2p(t,2\tau)\\
&\frac{dk}{dt}(t) = v(t)(1-k(t)) - \alpha k(t)\\
&\frac{\partial p}{\partial t}(t,a) + \frac{\partial p}{\partial a}(t,a) = -(\gamma + \chi_{(\tau,2\tau)}(a)u(t))p(t,a) \quad 0 < a < 2\tau\\
&p(t,0) = (1-k(t))\beta R(t)
\end{aligned}$$

In order to handle the transport equation for p, we note the total and second half proliferating populations

$$P(t) = \int_0^{2\tau} p(t,a)da, \quad P_2(t) = \int_\tau^{2\tau} p(t,a)da$$

As detailed in [13, 1], by the method of characteristics the dynamics can be rewritten as a system of delay differential equations corresponding to a controlled version of Mackey's model [28].

$$\begin{aligned}
\frac{dR}{dt}(t) = \quad & -(1-k(t))\beta R(t) + 2(1-k(t-2\tau)\beta R(t-2\tau)e^{-(\gamma 2\tau + \int_{t-\tau}^{\tau} u(s)ds)}\\
\frac{dP}{dt}(t) = \quad & -(\gamma P(t) + u(t)P_2(t)) + (1-k(t))\beta R(t)\\
& -(1-k(t-2\tau))\beta R(t-2\tau)e^{-(\gamma 2\tau + \int_{t-\tau}^{\tau} u(s)ds)}\\
\frac{dP_2}{dt}(t) = \quad & -(\gamma + u(t)P_2(t)) + (1-k(t-\tau))\beta R(t-\tau)e^{-\gamma\tau}\\
& -(1-k(t-2\tau))\beta R(t-2\tau)e^{-(\gamma 2\tau + \int_{t-\tau}^{\tau} u(s)ds)}\\
\frac{dk}{dt}(t) = \quad & v(t)(1-k(t)) - \alpha k(t)
\end{aligned}$$

We refer the reader to [13] for the formal analysis of this system, namely the existence of solutions and the introduction of age-weighted populations $\tilde{P}, \tilde{P}_2$ to counteract the horizon effect that would cause to always stop all treatment at the end of the time interval. Taking into account constraints on the maximal cumulative dose of drugs, the resulting optimal control problem writes as

$$\begin{cases} Min\ R(T) + \tilde{P}(T) \\ \frac{dR}{dt}(t) = -(1-k(t))\beta R(t) + \tilde{p}(t, 2\tau) \\ \frac{d\tilde{P}}{dt}(t) = \lambda \tilde{P}(t) - u(t)\tilde{P}_2(t) + \tilde{p}(t,0) - \tilde{p}(t, 2\tau) \\ \frac{d\tilde{P}_2}{dt}(t) = (\lambda - u(t))\tilde{P}_2(t) + \tilde{p}(t,\tau) - \tilde{p}(t, 2\tau) \\ \frac{dk}{dt}(t) = v(t)(1-k(t)) - \alpha k(t) \\ 0 \le u(t) \le \bar{u}, \quad 0 \le v(t) \le \bar{v} \\ \int_0^T u(t)dt \le \bar{U} \end{cases}$$

where λ is defined by the equation $\lambda + \beta = 2\beta e^{-(\lambda+\gamma)2\tau}$ and

$$\begin{array}{l} \tilde{p}(t,0) = (1-k(t))(\lambda+\beta)R(t) \\ \tilde{p}(t,\tau) = (1-k(t-\tau))(\lambda+\beta)R(t-\tau)e^{\lambda\tau} \\ \tilde{p}(t,2\tau) = (1-k(t-2\tau))(\lambda+\beta)R(t-2\tau)e^{\lambda 2\tau - y(t)} \\ y(t) = \int_{t-\tau}^{t} u(s)ds \end{array}$$

with the border cases

$$\begin{array}{ll} \tilde{p}(t,\tau) = p_0(\tau - t)2e^{-\gamma t - (\lambda+\gamma)\tau} & \text{if } t < \tau \\ \tilde{p}(t,2\tau) = p_0(2\tau - t)2e^{-\gamma t - y(t)} & \text{if } t < 2\tau \\ y(t) = \int_0^t u(s)ds & \text{if } t < \tau \end{array}$$

From [13] we take the initial conditions

$$R(0) = R_0 = 4\ 10^5,\ k(0) = 0,\ y(0) = 0,$$

$$\tilde{P}(0) = \int_0^{2\tau} e^{(\lambda+\gamma)(a-2\tau)} p_0(a)da, \quad \tilde{P}_2(0) = \int_\tau^{2\tau} e^{(\lambda+\gamma)(a-2\tau)} p_0(a)da.$$

and the parameters

$$T = 5,\ \tau = 1,\ p_0(a) = 0.5\ 10^5,\ \alpha = 1,\ \beta = 2,\ \bar{v} = 2,\ \gamma = 0.05.$$

Numerical simulations are carried out for three cases: $\bar{u} = 0.2$, $\bar{U} = 2\bar{u}$ (Fig. 19); $\bar{u} = 1$, no limit $\bar{U}$ (Fig. 20); and $\bar{u} = 1$, $\bar{U} = 2\bar{u}$ (Fig. 21).

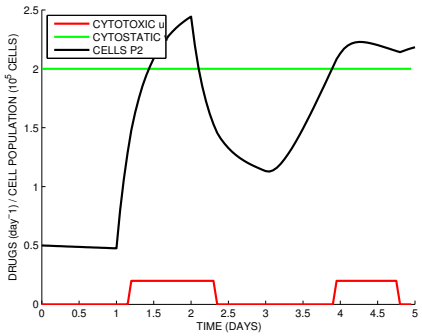

Figure 19: Low cytotoxic dose $\bar{u} = 0.2$, with cumulative limit. Optimal solution is bang-bang with cytotoxic administered when sub-population P_2 is high.

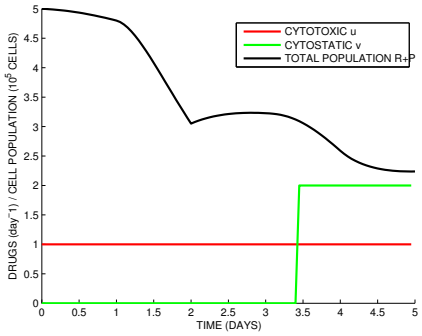

Figure 20: High cytotoxic dose $\bar{u} = 1$, without cumulative limit. Optimal cytostatic is bang-bang.

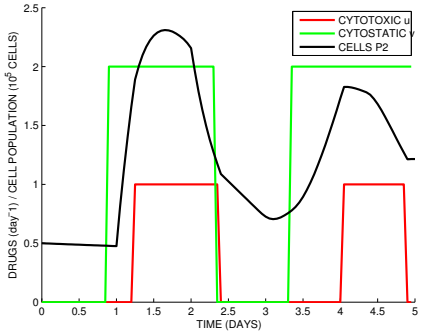

Figure 21: High cytotoxic dose $\bar{u} = 1$, with cumulative limit. Both optimal cytostatic and cytotoxic are bang-bang.

5 Energy systems

5.1 Energy management for an electric microgrid

We present here a microgrid problem introduced and solved by MILP techniques in [30], later studied in [22] with direct and Hamilton-Jacobi-Bellman methods. In the context of an isolated village in the Chilean mountains, we consider a microgrid comprised of a diesel generator, photo-voltaic panels and a battery energy storage system (BESS). The aim is to satisfy the energy demand (power load) from the villagers at all times, while minimizing the overall diesel consumption. One of the difficulties is that the diesel generator has a turn-on cost, thus we have to keep track of its on/off state over time. This problem falls in the class of switched systems and can be solved with a dynamic programmning approach.

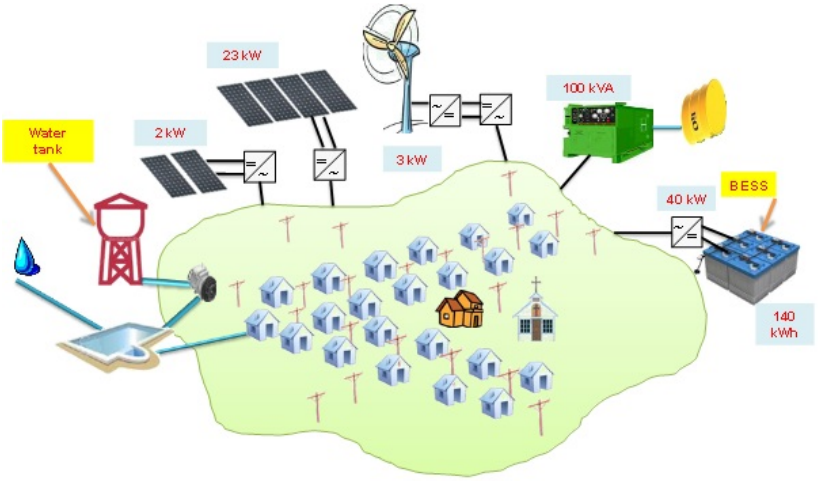

We consider a fixed horizon $T = 48$ hours. For $t \in [0, T]$, we denote by $P_S(t)$ the solar power from the photovoltaic panels, $P_D(t)$ the diesel generator power and $P_L(t)$ the electricity load.

Dynamics. The state of charge $SOC(t)$ of the BESS evolves according to

$$\dot{SOC}(t) = \frac{1}{Q_B}\left(P_I(t)\rho_I - P_O(t)/\rho_O\right) = \frac{1}{\tilde{Q}_B}\left(P_I(t)\tilde{\rho} - P_O(t)\right)$$

where Q_B is the maximum capacity of the battery, $P_I, P_O > 0$ are the input and output power of the BESS, and ρ_I, ρ_o are the efficiency ratios for the charge and discharge processes, assumed constant. We introduce the slack variable P_{slack} that represents the excess power ($P_{slack} < 0$), which has to be shed, or the missing power in the microgrid ($P_{slack} > 0$), which turns into unmet demand. The addition of this variable ensures the mathematical feasibility of the problem.

Cost function. We model the fuel consumption of the diesel generator by

$$\int_0^T K P_D(t)^{0.9} dt, \quad K = 0.471.$$

The fuel consumption curve is strictly concave and was extrapolated from the datasheet provided by the diesel generator manufacturer as in [30]. Note that turning the diesel generator on adds a fixed instantaneous consumption of $2l$. Total cost is the sum of the diesel cost and unserved energy cost $C_{US}P^+_{slack}$, with $C_{US} = 1000CLP$ and the unit price for diesel $C_D = 500CLP$ (Chilean Pesos).

Constraints. For physical reasons, the system is subject to the following constraints at every time $t \in [0, T]$. These include the bounds for the battery state of charge, diesel generator power outptut, and discharge/charge limits for the BESS

$$\begin{cases} SOC(t) \in [0.2, 1], P_D(t) \in \{0\} \cup [5, 120], P_O(t) \in [0, 40], \\ P_I(t, P_D(t), P_{slack}) \in [0, 13.2] \quad \text{if } SOC(t) < 0.9, \\ P_I(t, P_D(t), P_{slack}) \leq 1320(1 - SOC(t))^2 \quad \text{otherwise.} \end{cases}$$

Moreover, the power equilibrium must hold at all times and can be used to eliminate some of the variables:

$$P_D + P_O + P_S + P_{slack} - P_L - P_I = 0.$$

External data. We choose two test cases of a 48h time frame in winter and summer. The power load P_L and solar power P_S are shown below.

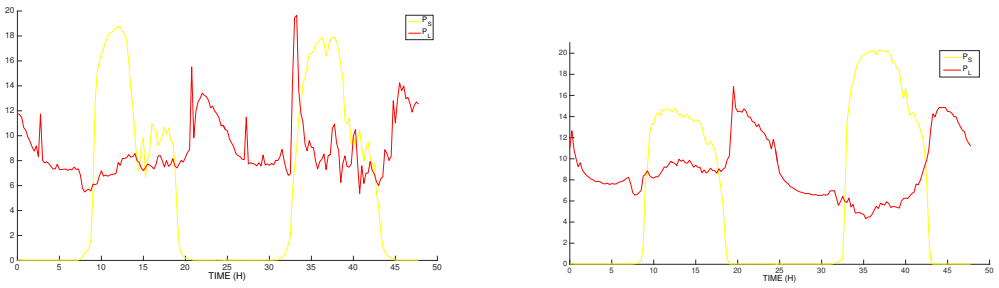

Power load and solar power for the two test cases (summer and winter)

The 'PMP trick'. This problem can be solved directly by BocopHJB using a basic control discretization for P_D and P_{slack}. However, in this particular case, we are able to exploit the properties of the problem to improve the method. If $\bar{u}$ is the optimal control, denote by $\bar{x}$ the optimal state and $\bar{p}$ the costate associated to the dynamics constraint $\dot{x}(t) = F(t, u(t))$. Defining the Hamiltonian $H(u, p, t) := pF(u, t) + \ell(u)$ the Pontryagin's Maximum Principle (PMP) says that for all $t \in [0, T]$ we have

$$H(\bar{u}(t), \bar{p}(t), t) \leq H(v, \bar{p}(t), t) \text{ for all } v \in U_{\bar{x}(t)}.$$

Since the dynamics is continuous and piecewise affine, the Hamiltonian is the sum of a continuous, piecewise affine and of a continuous strictly concave functions, and therefore is continuous, piecewise strictly concave. Therefore it can attain its minimum only at one of the extreme points of the pieces. Taking into account the constraints, we have at most five possible optimal controls, as illustrated below. Moreover, the values of these controls can be computed explicitly, since they do not depend on $\bar{p}$ (which is not true in general). Therefore, instead of the usual control discretization we only test these controls, gaining

both in speed and precision. So:
- if the Diesel is off (mode 0), we simply take $P_D = 0$.
- if the Diesel is on (mode 1), we test the five cases: $P_D = 5$ (minimum power),$P_D = 120$ (maximum power), P_D such that $\dot{SOC} = 0$ (battery unused), P_D such that $P_i = P_i^{max}(SOC)$ (maximal charge), and P_D such that $P_0 = 40$ (maximal discharge).

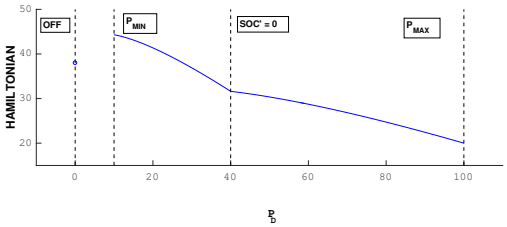

The PMP trick illustrated

We present the results of the optimization for the two test cases. The Solar Power fills the demand, with any excess power used to charge the battery. The Diesel is always off when solar power is available, and is switched on once a day during the evening peak in demand. The Diesel output is often greater than power demand: it is also used to charge the battery. The battery fills the gaps between production and demand especially at night.

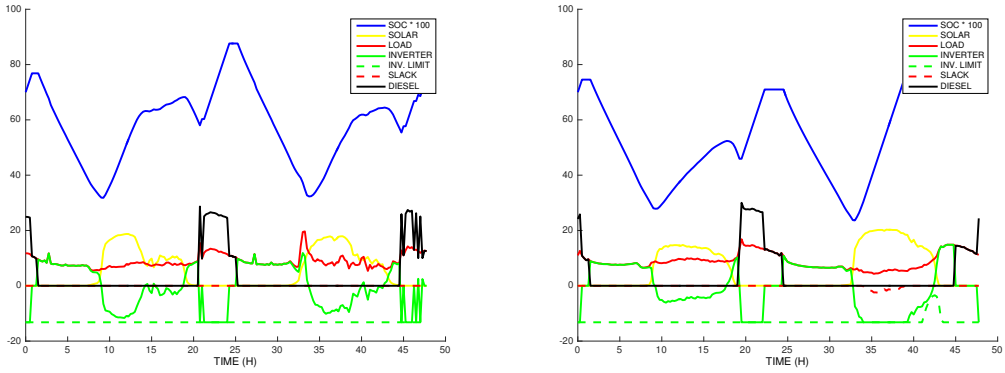

Solution for the two test cases (summer and winter)

Other formulations. We can also solve the problem using a manual control discretization for $P_D \in 0 \cup [6, 120]$. Finally, given the small number of admissible controls, we can actually model each of them with modes and remove the control P_D altogether. The solutions obtained by the different formulations are quite close, as summarized on Table 2.

	Discretization	PMP trick	Modes only
Diesel range	[10,30]	[9,30]	[9,28]
Switchings	2	2	2
Total Cost	32211	32197	31435
SOC range	[0.22,0.91]	[0.24,0.95]	[0.24,0.95]
Slack Range	[-3,0]	[-2.5,0]	[-2.5,0]
Cpu Time	3	1	1

Table 2: Microgrid: comparison of the three HJB formulations - Winter case

6 Mechanical systems, aerospace

6.1 Clamped beam [Bocop]

A classical example of second-order state constraint is the Euler-Bernoulli beam, see Bryson et al. [11]

$$
\begin{aligned}
&Min\ \tfrac{1}{2}\int_0^1 u(t)^2 dt \\
&\ddot{x}(t) = u(t) \\
&x(t) \leq a \\
&x(0) = x(1) = 0 \\
&\dot{x}(0) = -\dot{x}(1) = 1.
\end{aligned}
$$

The exact solution, for various values of a, is displayed in figure 22, and is such that
- if $a \geq 1/4$, the constraint is not active and the solution is $x(t) = t(1-t)$.
- if $a \in [1/6, 1/4]$, there is a touch point at $t = 1/2$.
- if $a < 1/6$, there is a boundary arc without strict complementarity: the measure has its support at end points. The locus of switching points is piecewise affine.

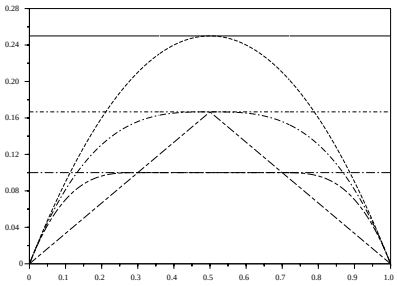

Figure 22: Shape of a beam: the three cases and the locus of junction points

The numerical results are consistent with the theory: we display in figure 23 the displacement and control when $a = 0.1$, with the expected boundary arc.

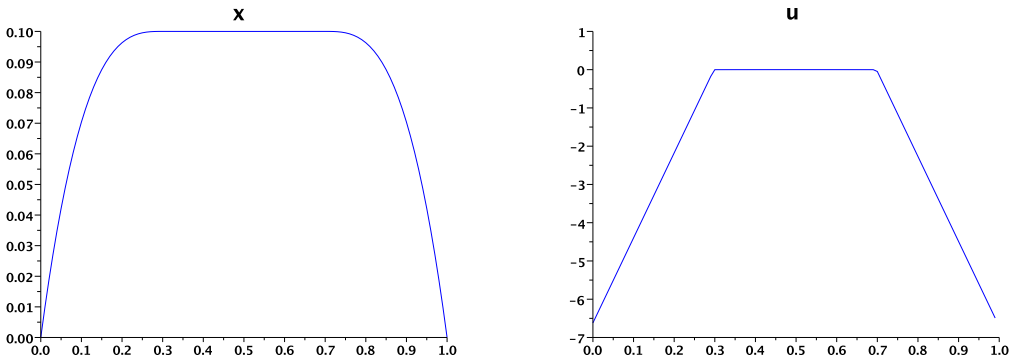

Figure 23: **beam:** state and control. Boundary arc case ($a = 0.1$).

6.2 Lagrange equations

We briefly recall the derivation of rational mechanics by the Lagrange approach [26]. Given generalized coordinates $q \in \mathbf{R}^N$, we note $E(q,\dot{q})$ and $U(q)$ the expression of cinetic and potential energy. The associated *Lagrangian function* and *action functional* are

$$L(q,\dot{q}) := E(q,\dot{q}) - U(q); \quad A(q,\dot{q}) := \int_0^T L(q(t),\dot{q}(t))dt. \tag{7}$$

The Lagrange equations are the Euler Lagrange equations of the classical calculus of variations, namely

$$0 = \frac{d}{dt}\frac{\partial L}{\partial \dot{q}} - \frac{\partial L}{\partial q} = \frac{d}{dt}\left(\frac{\partial E(q,\dot{q})}{\partial \dot{q}}\right) - \frac{\partial E(q,\dot{q})}{\partial q} + U'(q) \tag{8}$$

with $U'(q)$ the derivative of the potential function (opposite of the force deriving from the potential). The above relation must be understood as

$$\frac{d}{dt}\left(\frac{\partial E(q,\dot{q})}{\partial \dot{q}_i}\right) = \frac{\partial E(q,\dot{q})}{\partial q_i} - \frac{\partial U(q)}{\partial q_i}, \quad i = 1,\ldots,N. \tag{9}$$

The cinetic energy is usually of the form

$$E(q,\dot{q}) = \frac{1}{2}\dot{q}^\top M(q)\dot{q}, \tag{10}$$

where the $N \times N$ *mass matrix* $M(q)$ is symmetric, positive definite. Since $\frac{\partial E(q,\dot{q})}{\partial \dot{q}_i} = M(q)\dot{q}_i$, the Lagrangian equations gives

$$\frac{d}{dt}(M(q)\dot{q})_i = \frac{1}{2}(\dot{q})^\top \frac{\partial M(q)}{\partial q_i}\dot{q} - \frac{\partial U(q)}{\partial q_i}, \quad i = 1,\ldots,N. \tag{11}$$

For the simplest spring model, we have $E(q,\dot{q}) = \frac{1}{2}m\dot{q}^2$ and $U(q) = \frac{1}{2}kq^2$, where m and k are the mass and spring stiffness. The Lagrangian equations reduce to $m\ddot{q}(t) = -kq(t)$, as expected.

6.3 Holonomic constraints

A (vector) holonomic constraint $G(q) = 0$, with $G : \mathbf{R}^N \to \mathbf{R}^M$, generates (generalized) forces of the type $DG(q)^\top\lambda$, i.e., orthogonal to $KerDG(q)$. The simplest way to express the resulting equations is to apply the Euler-Lagrange equation to the "augmented" Lagrangian $L[\lambda](q,\dot{q}) := L(q,\dot{q}) + \lambda \cdot G(q)$. The resulting equations are

$$\begin{aligned} \frac{d}{dt}(M(q)\dot{q})_i &= \frac{1}{2}(\dot{q})^\top \frac{\partial M(q)}{\partial q_i}\dot{q} + \lambda \cdot \frac{\partial G(q)}{\partial q_i} - \frac{\partial U(q)}{\partial q_i}, \quad i = 1,\ldots,N & (12)\\ G(q) &= 0. & (13) \end{aligned}$$

This is an example of an algebraic differential system. The successive time derivatives of the algebraic constraint are

$$G^{(1)}(q) = DG(q)\dot{q}; \quad G^{(2)}(q) = D^2G(q)(\dot{q})(\dot{q}) + DG(q)\ddot{q} \tag{14}$$

Substituting the expression of $\ddot{q}$ in (12), we obtain

$$G^{(2)}(q) = DG(q)M(q)^{-1}D^{\top}G(q)\lambda + F(q,\dot{q}) = 0. \tag{15}$$

If $DG(q)$ is onto, and $M(q)$ is positive definite, then $DG(q)M(q)^{-1}D^{\top}$ is invertible, meaning that we can eliminate the algebraic variable λ from the algebraic equation (15). This is a highly desirable property for the numerical schemes, and hence, the reader is advised to use the second derivative of the holonomic constraint in the discretized problem, rather than the holonomic constraint itself.

Of course the intial condition $(q^0, \dot{q}^0)$ should be compatible with the holonomic constraint, i.e., it should satisfy

$$G(q^0) = G^{(1)}(q) = DG(q^0)\dot{q}^0 = 0. \tag{16}$$

6.4 Inverted pendulum [Bocop]

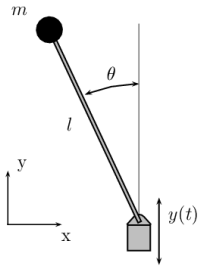

We study the pendulum problem to illustrate the use of algebraic variables. The inverted pendulum is governed by the equation $m\ddot{\theta} = g\sin\theta$ where θ is the angle to the vertical. The Lagrangian is $L = \frac{1}{2}m\dot{\theta}^2 - g\cos\theta$. Alternately, let (x, y) be the Cartesian coordinates of the position of the pendulum, subject to the constraint $G(x, y) = \frac{1}{2}(x^2 + y^2 - 1) = 0$. The Lagrangian is then

$$L = \frac{1}{2}(\dot{x}^2 + \dot{y}^2) + mgy + \frac{1}{2}\lambda(x^2 + y^2 - 1), \tag{17}$$

and the mechanical equations are

$$m\ddot{x} = \lambda x + u, \quad m\ddot{y} = \lambda y - mg. \tag{18}$$

where we have set an horizontal force as the control u.

We want to minimize the objective

$$Min \int_0^T x^2(t) + (y(t) - 1)^2 + \gamma u^2(t) \quad dt$$

Figure 24 shows the states x, y, the control u and multiplier λ. We take here $T = 12$, $m = 1$, $g = 1$ and $\gamma = 1$, with the boundary conditions $x(0) = -0.4794255$, $y(0) = 0.8775826$, $\dot{x}(0) = 1.0530991$, $\dot{y}(0) = 0.5753106$ and $x(T) = 0$, $y(T) = 1$, $\dot{x}(T) = 0$, $\dot{y}(T) = 0$.

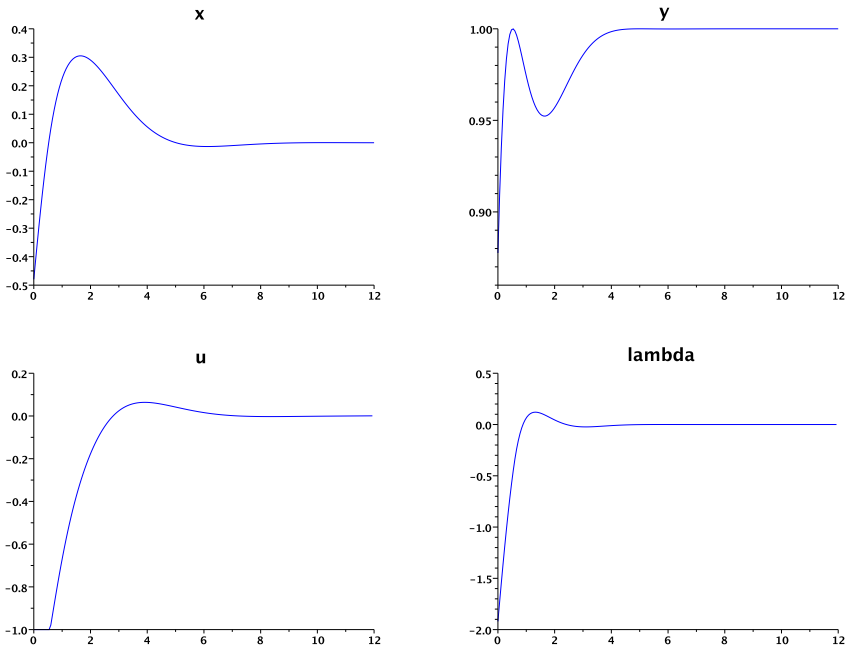

Figure 24: **pendulum:** state x, y, control u and multiplier λ.

6.5 Car with obstacle [BocopHJB]

We consider here a model for a very simplified car. The state variables x and y are the coordinates of a pointlike car in $\mathbb{R}^2$. The control coordinates u and θ correspond respectively to the velocity and the direction of the car. Then the dynamics is

$$\dot{x} = u\cos\theta, \dot{y} = u\sin\theta$$

We want to reach a prescribed position as fast as possible, so the objective is

$$\min \int_0^T f(x(t), y(t))dt$$

where $f(x, y)$ is 0 if we are close enough to $(x_f, y_f) = (0.2, 0.75)$, and 1 else. We define the part of the space where the car can go in order to illustrate the use of state contraints with BocopHJB. First x and y are both in [0,1]. In addition, we consider a forbidden zone defined by the constraints

$$\{(x, y) : x < 0.5, 0.25 + 0.5x < y < 0.75 - 0.5x\}$$

Figure 25 shows the value function we get, with the simulated trajectory for the initial conditions $(x_0, y_0) = (0.2, 0.2)$.

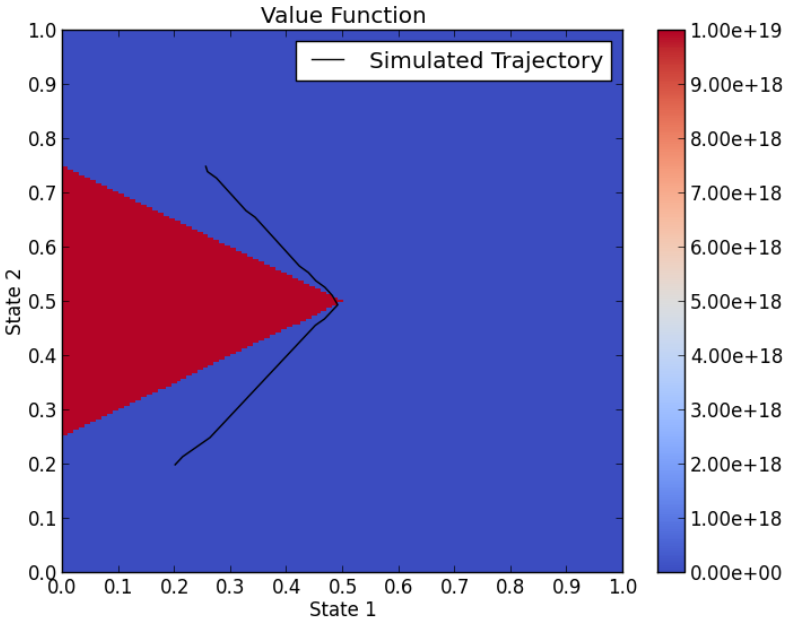

Figure 25: **car:** value function and simulated trajectory.

6.6 Goddard problem [Bocop]

This well-known problem (see for instance [17, 34]) models the ascent of a rocket through the atmosphere, and we restrict the study to vertical (monodimensional) trajectories. The state variables are the altitude, speed and mass of the rocket during the flight. The rocket is subject to gravity, thrust and drag forces. The final time is free, and the objective is to reach a certain altitude with a minimal fuel consumption, ie a maximal

final mass. The optimal control problem is written as (all units are renormalized)

$$\begin{cases} \max\ m(T) \\ \dot{r} = v \\ \dot{v} = -\frac{1}{r^2} + \frac{1}{m}(T_{max}u - D(r,v)) \\ \dot{m} = -bu \\ u(\cdot) \in [0,1] \\ r(0) = 1,\ v(0) = 0, m(0) = 1 \\ r(T) = 1.01 \\ D(r(\cdot), v(\cdot)) \leq C \\ T\ free \end{cases}$$

The expression of the drag force is

$$D(r,v) = Av^2\rho(r),\ \text{with the volumic mass } \rho(r) = e^{-k(r-r0)}.$$

Control structure and state constraint

The Hamiltonian is an affine function of the control, so singular arcs may occur. We consider here a path constraint limiting the value of the drag effect $D(r,v) \leq C$, to model some kind of structural limit of the rocket. We will see that depending on the value of C, the control structure changes. In the unconstrained case, the optimal trajectory presents a singular arc with a non-maximal thrust. When C is set under the maximal value attained by the drag in the unconstrained case, a constrained arc appears. If C is small enough, the singular arc is completely replaced by the constrained arc. These different structures are illustrated on Fig.26, with the parameters $b = 7$, $T_{max} = 3.5$, $A = 310$, $k = 500$ and $r0 = 1$.

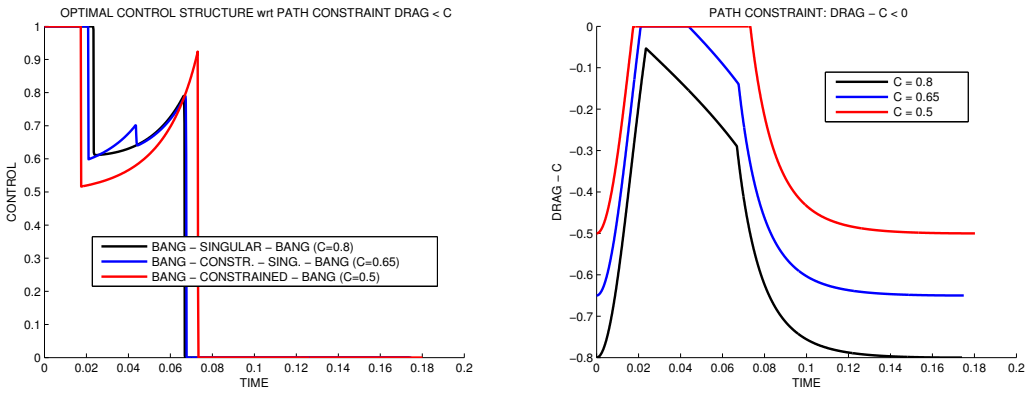

Figure 26: **goddard**: control structure is BSB, BCSB or BCB depending on the severity of the drag path constraint.

6.7 3-Link Purcell micro-swimmer [Bocop]

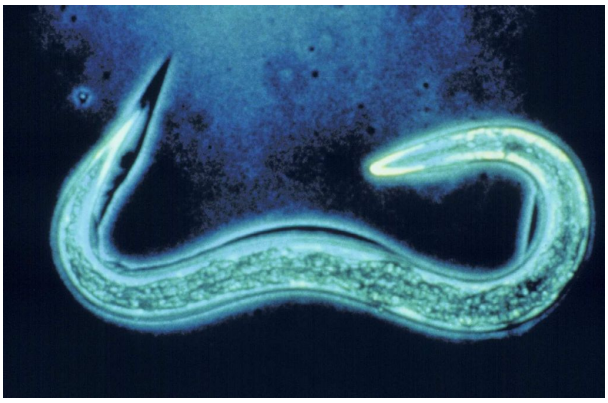

A nematode microscopic worm

The study of optimal swimming strategies at the microscopic scale draws interest from both fields of biological and robotic systems. In [15, 16] we study the so-called N-link swimmer, more precisely the 3-link swimmer introduced by Purcell in [32].

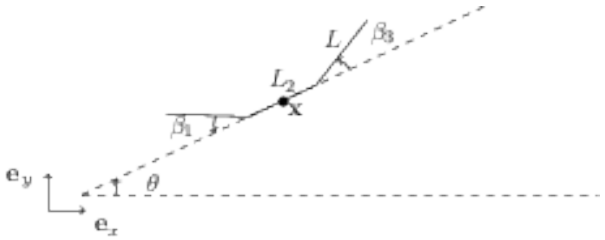

Purcell's 3-link swimmer

Swimming at low Reynolds number, Resistive Force Theory
At the microscopic scale, the situation is the one of low Reynolds numbers, with inertial forces neglected compared to viscosity. Therefore the hydrodynamics of the system are governed by the Stokes equation, and the dynamics of the swimmer follow the Newton laws without inertia. The Resistive Force Theory ([19]) provides a local drag approximation, assuming that the force exerted on the swimmer by the fluid is linear with respect to velocity. In this framework, the dynamics of the N-link swimmer in a plane can be expressed as follows, noting (x, y, θ) the position and orientation of the swimmer, and β_i the shape angles between two adjacent links:

$$\begin{pmatrix} \dot{x}_1 \\ \dot{y}_1 \\ \dot{\theta}_1 \end{pmatrix} = \sum_{i=1}^{N-1} \left(g_i \left(\theta_1, \beta_2, \cdots, \beta_N \right) \right) \dot{\beta}_{i+1}$$

We observe that the dynamics has no drift term, meaning that without deformation of its shape, the swimmer remains motionless. The actual expression of the g_i can be found in [16].

Optimal swimming problem
Noting the state $z = (x, y, \theta)$ and the control $u = \dot{\beta}$, we can formulate the optimal

swimming problem for different objective functions (maximal displacement, minimum time, minimum work, ...).

$$(OCP)\begin{cases} Min\ J(z,u) \\ \dot{z} = f(z,u) \\ \dot{\beta} = u \in [-b,b]^N \\ \beta \in [-a,a]^N \end{cases}$$

Simulations: maximal displacement along x-axis
We solve the above problem while maximizing horizontal displacement, with no a priori assumption on periodicity. We observe on Fig.27 that the optimal trajectory is indeed a sequence of periodic strokes, different from the classical Purcell strokes. More precisely, the state constraints on the shape angles are active and the control structure has both bang and constrained arcs. The optimal stroke appears to be shorter (in time) than the classical Purcell stroke, see Fig.28.

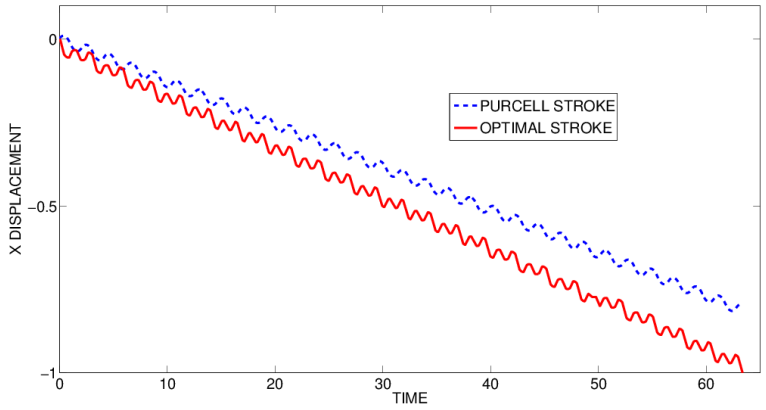

Figure 27: **purcell:** comparison of Purcell and optimal strokes

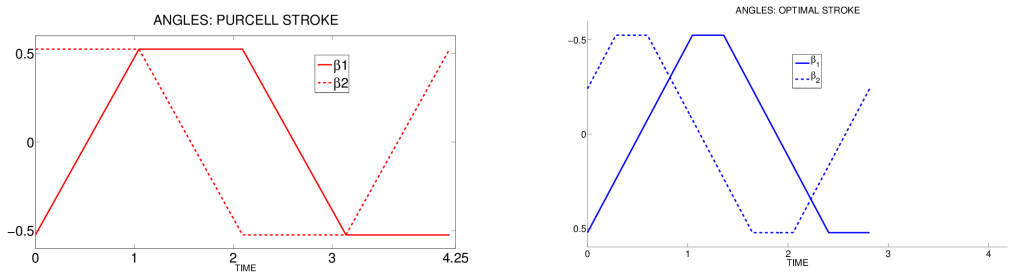

Figure 28: **purcell:** deformation of shape angles β_1, β_2 along time

Micro-swimmer optimal design
In [16] we address the question of the optimal length for each link, in order to maximize the displacement of the swimmer. The classical Purcell swimmer is defined by $L_1 = L_3 = L = 1, L_2 = 2$, meaning the central link is twice as long as the other two. Assuming an

octagonal-shaped stroke (in the (β_1, β_2) plane), we use an asymptotic expansion of the displacement for small amplitudes to derive the optimal ratio

$$\left(\frac{L_2}{L}\right)^* = \frac{\sqrt{10}-1}{3} \sim 0.721$$

For a total length of 4 this corresponds to $L^* = 1.4702, L_2^* = 1.0596$. Numerical simulations give results quite close to these values, and show a gain in displacement about 60% versus the traditional Purcell swimmer. We show below the comparison between the Purcell swimmer and the optimal swimmer for an amplitude $a = \pi/6$ and different deformation speed limits b.

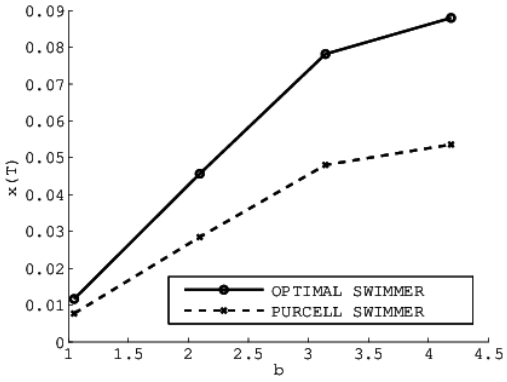

Purcell vs optimal swimmer for different speed limits b

Finally, if we set the speed limit to $b = 1$ and solve the problem for different amplitudes a, we observe a change in the stroke phase portrait. For large amplitudes, we obtain unconstrained solutions instead of octagonal shapes. These solutions typically have a control structure with bang and singular arcs (instead of constrained arcs).

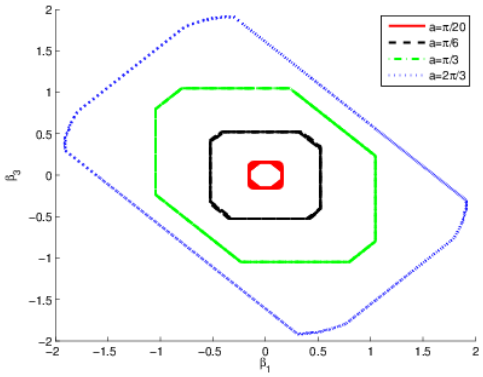

Phase portrait for different amplitudes, including an unconstrained solution (most exterior one)

7 PDE control of parabolic equations

The space discretization of parabolic equations allows to obtain large scale, stiff ODE models for which an implicit Euler scheme is well suited. In the case of complex geometries, one should import the dynamics from finite elements libraries such as FreeFem (available on FreeFem.org). Relevent references on this subject are Barbu [4], Hinze et al. [23], Tröltzsch [35], and of course the pioneering book by J.L. Lions [27].

7.1 Control of the heat equation [Bocop]

We next give a simple example for the one dimensional heat equation, over the domain $\Omega = [0, 1]$. We set $Q = \Omega \times [0, T]$, where the final time is fixed. The control $u(t)$ is either over a part of the domain, with Dirichlet conditions, or at the boundary by the Neumann condition. So the state equation is in the Dirichlet case

$$\frac{d}{dt}y(x,t) - c_0\ y_{xx}(x,t) = \chi_{[0,a]}c_1\ u(t), \quad (x,t) \in Q, \tag{19}$$

$$y(\cdot,0) = y_0(x); \quad y(0,t) = y(1,t) = 0, \quad t \in [0,T], \tag{20}$$

where $0 < a \leq 1$, and $\chi_{[0,a]}$ is the characteristic function of $[0, a]$, and in the Neumann case

$$\frac{d}{dt}y(x,t) - c_0\ y_{xx}(x,t) = 0, \quad (x,t) \in Q, \tag{21}$$

$$y(\cdot,0) = y_0(x); \quad y_x(0,t) = -c_1 u(t); \quad y_x(1,t) = 0, \quad t \in [0,T]. \tag{22}$$

The cost function is, for $\gamma \geq 0$ and $\delta \geq 0$:

$$\frac{1}{2}\int_Q y(x,t)^2 dxdt + \int_0^T \left(\gamma u(t) + \delta u(t)^2\right) dt. \tag{23}$$

We discretize in space by standard finite difference approximations.

As an example, we take 50 space variables, with $c_0 = 0.02$, $c_1 = 20$, and a final time T=20. The discretization method is implicit Euler with 200 steps, and we set $\gamma = \delta = 0$, which gives a singular arc for the control. We display on Fig.29 the results in the case of the Dirichlet boundary condition ($a = 0$), while Fig.30 shows the Neumann case (with $c_0 = 0.2$). We can clearly see the differences between the boundary conditions $y(1, t) = 0$ and $y_x(1, t) = 0$.

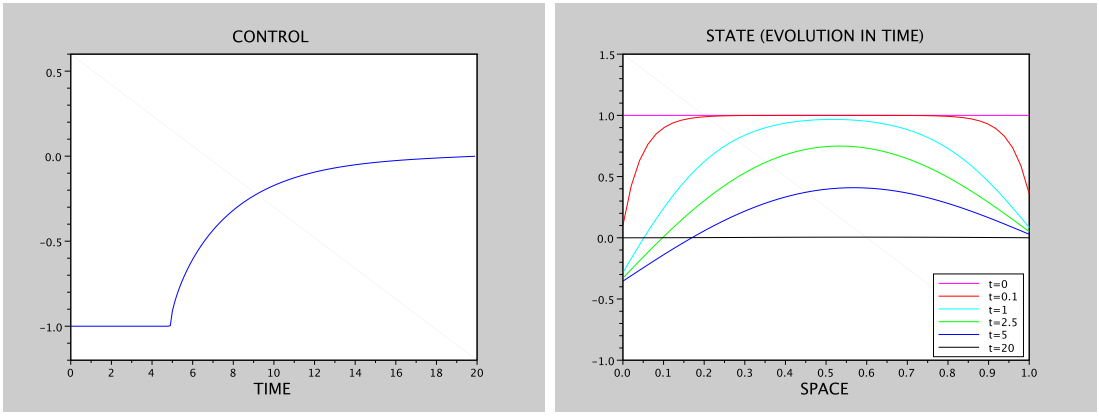

Figure 29: **heat:** Dirichlet condition, $u(t)$ and $y(\cdot, t)$.

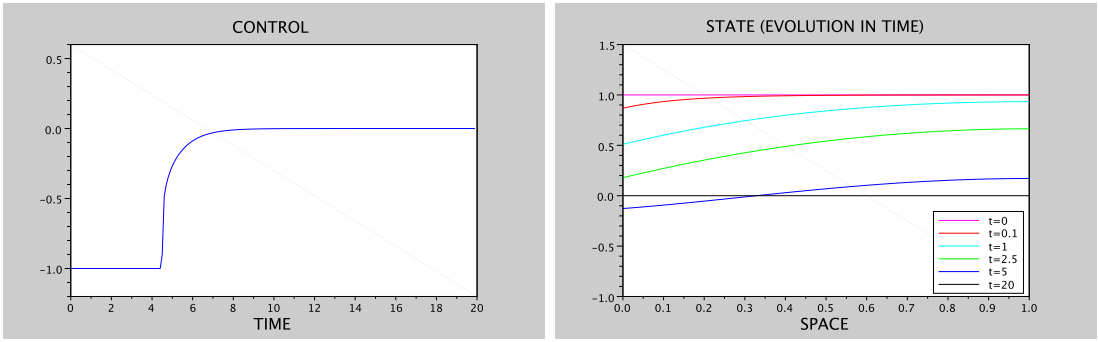

Figure 30: **heat:** Neumann condition, $u(t)$ and $y(\cdot, t)$.

8 Delay systems

See also 4.2 p.17.

8.1 A simple resource harvest problem (delay) [Bocop]

We study here the delay problem studied in [8, 18], originating from [29]. The aim is to find the optimal harvesting of a renewable ressource whose growth follows a logistic function. Denoting x the biomass of population and u the harvesting effort, the optimal control problem is stated as

$$\begin{cases} Min \ \int_0^T e^{-\beta t}(C_E \frac{u(t)^3}{x(t)} - pu(t))dt + 0.1T^2 \\ \dot{x} = ax(t)(1 - \frac{x(t-h)}{b}) - u(t) \\ x(t) = 2 \ \forall t \in [-h, 0] \quad , \quad x(t) \geq 2 \ \forall t \in [0, T] \\ u(t) \geq 0 \ \forall t \in [0, T] \\ T \ free. \end{cases}$$

with the harvesting cost $C_E = 0.2$, the growth rates $a = 3, b = 5$, the discount rate $\beta = 0.05$ and market price $p = 2$, and the growth delay $h = 0.5$.

Bocop can handle the delayed term $x(t - h)$ without having to perform the classical Guinn transformation [20], but for a fixed final time only. Therefore we perform a batch of optimizations for $T \in [1, 20]$, and iterate the process for $T \in [11, 13]$ to find a better estimate of the optimal time. Batch optimizations indicate an optimal final time $T^* \approx 12.24$ with an objective $J^* = -26.15$. Fig.31 represents the cost function for different final times T, and Fig.32 shows the optimal state and control for $T = 12.24$. These results are consistent with the solution presented in [8].

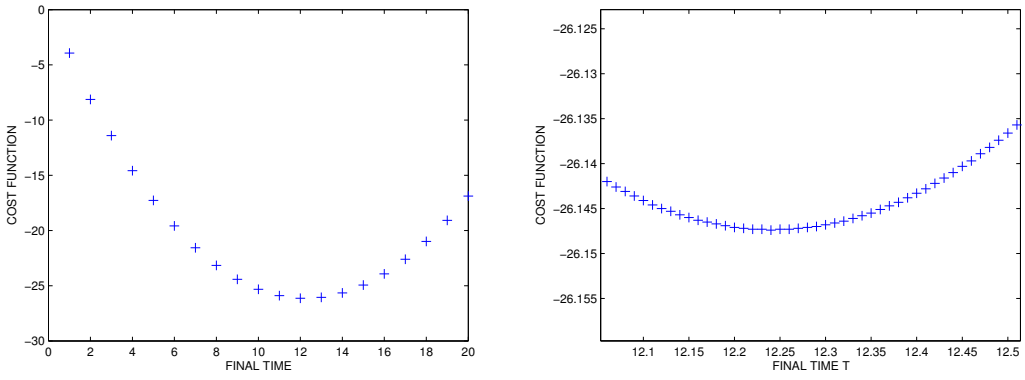

Figure 31: Delay problem. Cost function with respect to final time T.

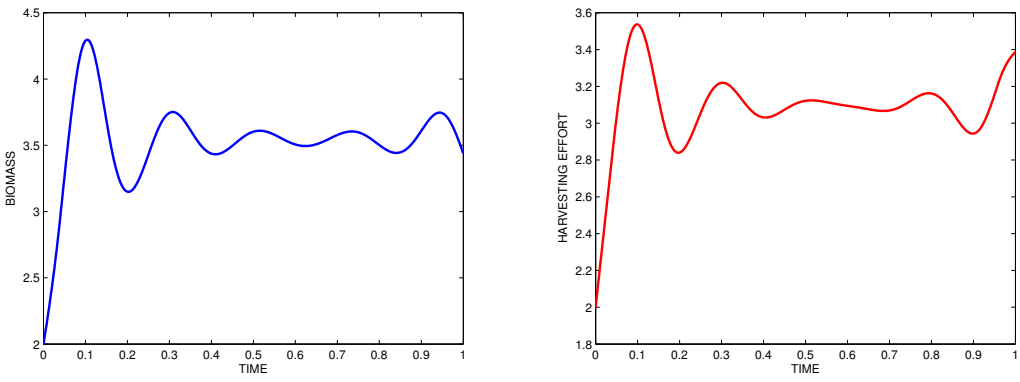

Figure 32: Delay problem. Optimal state and control for $T = 12.24$.

9 Switched systems

See also 5.1 p.20.

9.1 Thermostat [BocopHJB]

Here is an example of a system that can switch between different modes. We use a very simple thermostat system. The state x represents the temperature in the room. There is no control, only two modes corresponding to the heater being on or off. The dynamics of the thermostat is

$$\dot{x} = +10 \quad \text{when the heater is on}$$
$$\dot{x} = -10 \quad \text{when the heater is off.}$$

We define the objective as follows: there is no cost when the heater is off, and we have a constant cost of 1 per unit of time when the heater is on. We also have a switching cost of 1 when turning the heater on, and we set an additional cost of 10 per unit of time when the temperature goes below 50.

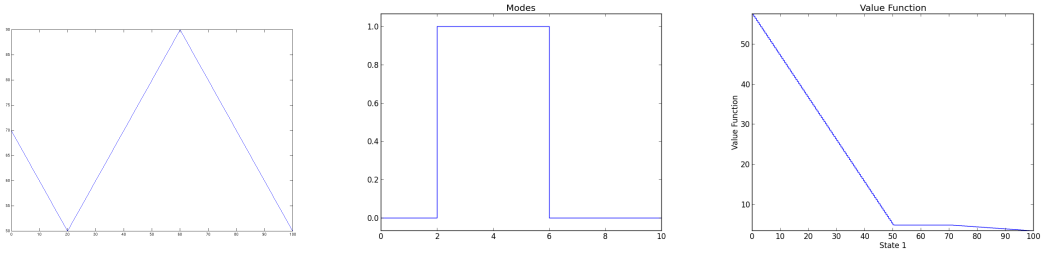

Figure 33: **thermostat:** simulated trajectory (state, mode) and value function $V(., t_0)$.

9.2 Mouse & Maze [BocopHJB]

To illustrate the use of both several switching possibilities and controls, we designed the following maze problem. A mouse trapped in a maze tries to get out. This mouse has a "bomberman" control space. The state can be described with the variable $(x, y) \in \mathbb{R}^2$ which defines the position of the unlucky pointlike mouse. The mouse has 4 modes modeling its direction: north, south, east, west. In addition to the direction modes, the mouse has a control variable for its velocity, which is positive and upper-bounded. We consider a running cost of 10 per unit of time in the maze, and each change of direction costs 1 as a switching cost. The mouse starts at the triangle center while the exit of the maze is at the green square. We show on Fig. 34 the optimal trajectories with unrestricted turns, and when allowing only counterclockwise or clockwise turns. The objective is 18.5 (unrestricted turns) versus 20.5 (counterclockwise turns) and 21.5 (clockwise turns).

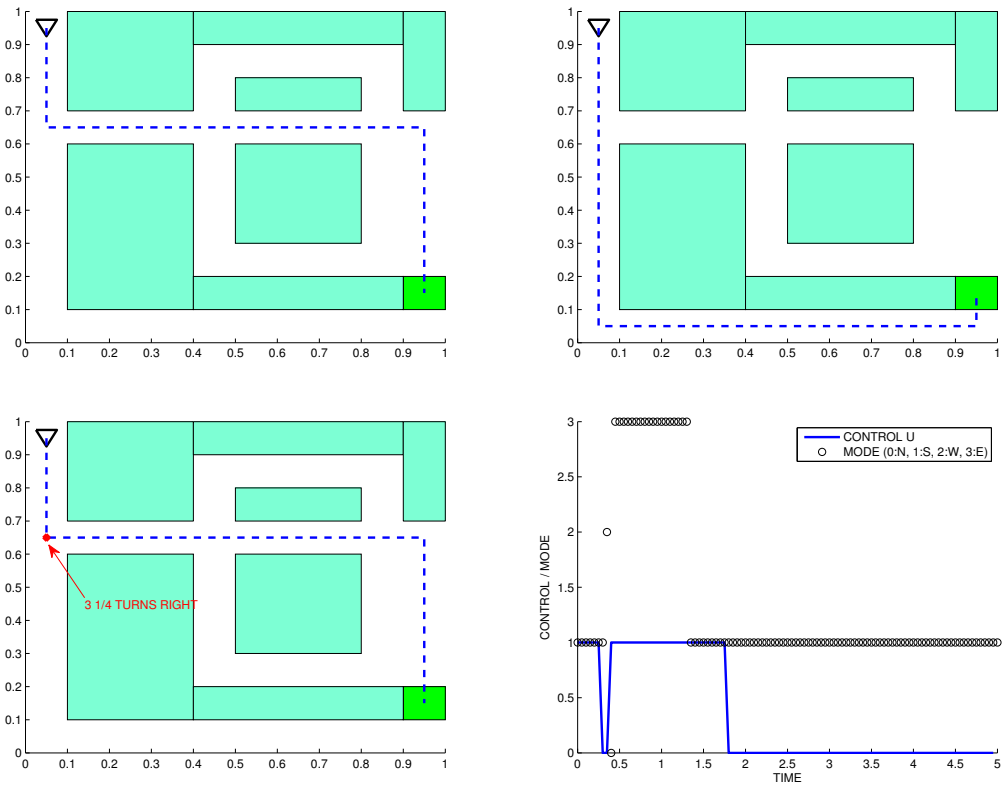

Figure 34: **maze:** the mouse & maze trajectory, with unrestricted and counter-clockwise turns. Below, the clockwise turns case, with its control and mode: what looks like a 'left' turn is actually a sequence of 3 turns to the right with null speed.

10 Stochastic applications in finance

10.1 Call option

We use the Black-Scholes model as an example of a stochastic problem without control variables. We compute the price of a European call option, with S the price of a stock as the state variable. In the Black-Scholes model, S follows the dynamics

$$dS = S(\mu dt + \sigma dW)$$

and the payoff is given by $g(S) = (S-K)^+ \, e^{-rT}$ where K is the strike and the interest rate is r. We solve Black-Scholes equation to compute the value of the option. We show on Fig. 35 the results for $r = 0.05$, $\sigma = 0.2$, $K = 105$, $T = 1$, $S_0 = 100$. We check that the value function is quite close to the explicit solution given by the Black-Scholes formula.

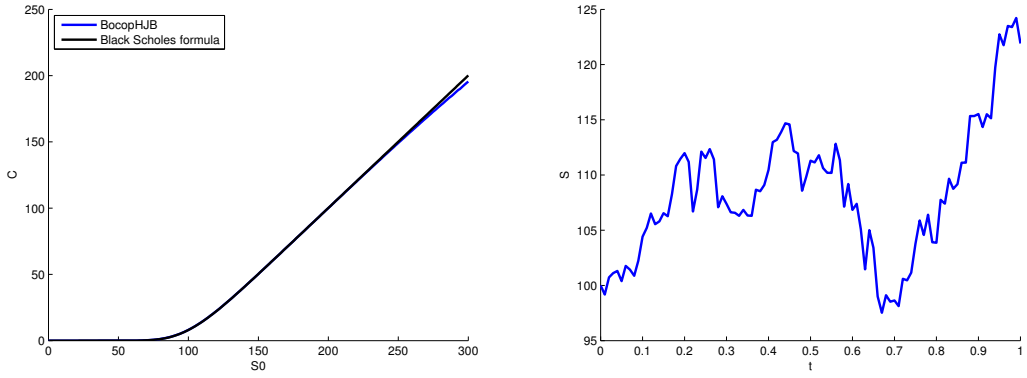

Figure 35: **option:** the price of a call option, computed with BocopHJB and with explicit formula (left), and an example of simulated trajectory (right)

Remark: we recall that for a call option the Black-Scholes formula gives the solution

$$\begin{aligned} C(S,t) &= N(d_1)S - N(d_2)Ke^{-r(T-t)} \\ d_1 &= \frac{1}{\sigma\sqrt{(T-t)}}(\ln(\frac{S}{K}) + (r + \frac{\sigma^2}{2})(T-t)) \\ d_2 &= d_1 - \sigma\sqrt{T-t} \end{aligned}$$

where N is the cumulative standard normal distribution function.

10.2 Portfolio allocation

As an example of a stochastic control problem, we consider the Merton portfolio allocation problem in finite horizon, for which the solution is known (see for instance [31]). The portfolio consists in a risky asset whose value S follows $dS = S(\mu dt + \sigma dW)$ and a non-risky asset whose value S_0 follows $dS_0 = S_0 r dt$. The portfolio is invested in the risky asset with proportion α, and the value of the portfolio X is the state variable with dynamics

$$dX_t = \frac{X_t \alpha_t}{S_t} dS_t + \frac{X_t(1-\alpha_t)}{S_t^0} dS_t^0 = X_t(\alpha_t \mu + (1-\alpha_t)r)dt + X_t \alpha_t \sigma dW_t.$$

We want to solve the utility maximization problem $\sup_\alpha \mathbb{E}(U(X_T^{x,\alpha}))$, where U is the CRRA utility function defined by $U(x) = \frac{x^p}{p}$. In this particular case we have the explicit expression of the value function

$$V(t,x) = e^{\rho(T-t)}U(x), \quad \text{with } \rho = \frac{(\mu - r)^2 p}{2\sigma^2(1-p)} + rp$$

and the optimal control is constant, equal to

$$\hat{\alpha} = \frac{\mu - r}{\sigma^2(1-p)}$$

We solve the problem for $T = 1, X_0 = 1, X \in [0, 10], \alpha \in [-1, 1]$ with the parameters $r = 1, \mu = 1.1, \sigma = 1, p = 0.5$. The discretization uses 500 steps for the time, 500 steps for the state, 200 steps for the control, and the results are displayed in Fig 36-37.

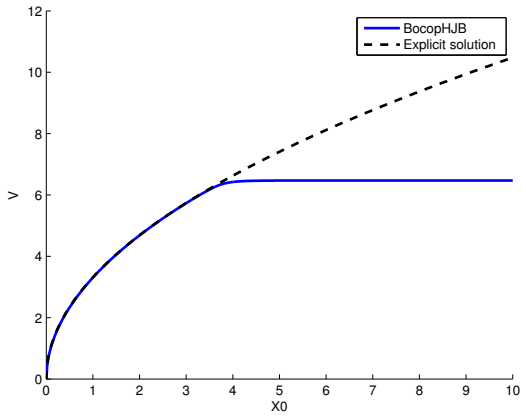

Figure 36: **portfolio (BocopHJB):** value function V. Discrepancy from theoretical solution for higher X_0 comes from the upper bound imposed on X by the state discretization.

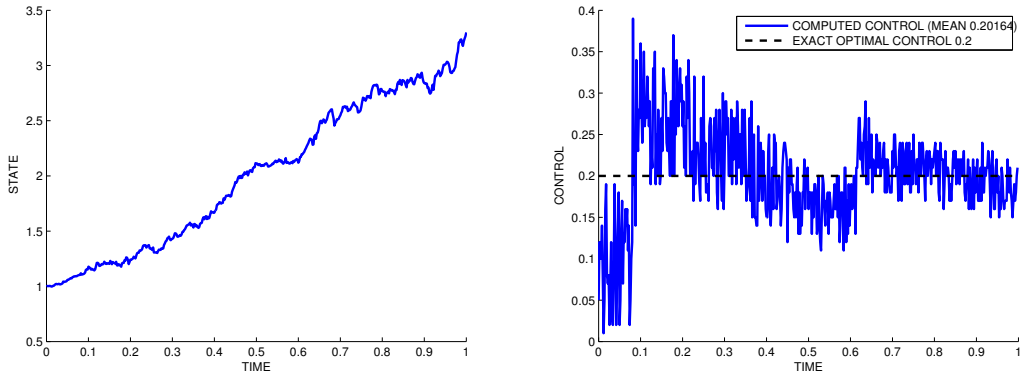

Figure 37: **portfolio (BocopHJB):** simulated trajectory (X, α). The mean of the computed control is quite close to $\hat{\alpha} = 0.2$.

References

[1] M. Adimy, F. Crauste, and A. El Abdllaoui. Discrete maturity-structured model of cell differentiation with applications to acute myelogenous leukemia. *J. Biol. Systems*, 16(3):395–424, 2008.

[2] G.M. Aly. The computation of optimal singular control. *International Journal of Control*, 28(5):681–688, 1978.

[3] S. Aronna, J.F. Bonnans, and P. Martinon. A well-posed shooting algorithm for optimal control problems with singular arcs. *J. Optim. Theory Appl.*, 2013. Online First, Jan. 2013.

[4] Viorel Barbu. *Analysis and control of nonlinear infinite-dimensional systems*, volume 190 of *Mathematics in Science and Engineering*. Academic Press Inc., Boston, MA, 1993.

[5] T. Bayen, F. Mairet, P. Martinon, and M. Sebbah. Analysis of a periodic optimal control problem connected to microalgae anaerobic digestion. *Optimal Control Applications and Methods*, 2014.

[6] Térence Bayen, Francis Mairet, Pierre Martinon, and Matthieu Sebbah. Optimizing the anaerobic digestion of microalgae in a coupled process. In *13th European Control Conference*, Zurich, Switzerland, 2013.

[7] L.T. Biegler. *Nonlinear programming*, volume 10 of *MOS-SIAM Series on Optimization*. Society for Industrial and Applied Mathematics (SIAM), Philadelphia, PA, 2010. Concepts, algorithms, and applications to chemical processes.

[8] A Boccia, P Falugi, H Maurer, and RB Vinter. Free time optimal control problems with time delays. pages 520–525. IEEE, 2013.

[9] B. Bonnard, M. Claeys, O. Cots, and P. Martinon. Comparison of Numerical Methods in the Contrast Imaging Problem in NMR. In *52nd IEEE Conference on Decision and Control*, Firenze, Italy, 2013.

[10] B. Bonnard, M. Claeys, O. Cots, and P. Martinon. Geometric and numerical methods in the contrast imaging problem in nuclear magnetic resonance. *Acta Applicandae Mathematicae*, pages 1–41, 2015.

[11] A.E. Bryson, W.F. Denham, and S.E. Dreyfus. Optimal programming problems with inequality constraints I: necessary conditions for extremal solutions. *AIAA Journal*, 1:2544–2550, 1963.

[12] Olivier Cots. *Contrôle optimal géométrique: méthodes homotopiques et applications*. PhD thesis, 2012.

[13] X. Dupuis. Optimal control of leukemic cell population dynamics. *Math. Model. Nat. Phenom.*, 9(1):4–26, 2014.

[14] A.T. Fuller. Study of an optimum non-linear control system. *J. of Electronics and Control*, 15:63–71, 1963.

[15] Laetitia Giraldi, Pierre Martinon, and Marta Zoppello. Controllability and Optimal Strokes for N-link Micro-swimmer. In *52nd IEEE Conference on Decision and Control*, Firenze, Italy, 2013.

[16] Laetitia Giraldi, Pierre Martinon, and Marta Zoppello. Optimal design of purcell's three-link swimmer. *Phys. Rev. E*, 91:023012, Feb 2015.

[17] R.H. Goddard. *A Method of Reaching Extreme Altitudes*, volume 71(2) of *Smithsonian Miscellaneous Collections*. Smithsonian institution, City of Washington, 1919.

[18] L. Goellmann, D. Kern, and H. Maurer. Optimal control problems with delays in state and control variables subject to mixed control-state constraints. *Optimal Control Applications and Methods*, 30(4):341–365, 2009.

[19] J. Gray and J. Hancock. The propulsion of sea-urchin spermatozoa. *Journal of Experimental Biology*, 1955.

[20] T. Guinn. Reduction of delayed optimal control problems to non-delayed problems. *Journal of Optimization Theory and Applications*, 18(3):371–377, 1976.

[21] Audrey Hermant. *Sur l'algorithme de tir pour les problèmes de commande optimale avec contraintes sur l'état*. PhD thesis, Ecole Polytechnique X, 2008.

[22] Benjamin Heymann, J. Frédéric Bonnans, Pierre Martinon, Francisco J. Silva, Fernando Lanas, and Guillermo Jiménez-Estévez. Continuous optimal control approaches to microgrid energy management. *Energy Systems*, 2017.

[23] M. Hinze, R. Pinnau, M. Ulbrich, and S. Ulbrich. *Optimization with PDE constraints*, volume 23 of *Mathematical Modelling: Theory and Applications*. Springer, New York, 2009.

[24] R. Jackson. Optimal use of mixed catalysts for two successive reactions. *J. Optimization Thery Applications*, 2(1):27–39, 1968.

[25] D.H. Jacobson, M.M. Lele, and J.L. Speyer. New necessary conditions of optimality for control problems with state-variable inequality contraints. *J. of Mathematical Analysis and Applications*, 35:255–284, 1971.

[26] J.-L. Lagrange. *Mécanique analytique*. Paris, 1788. Reprinted by J.Gabay, 1989.

[27] J.-L. Lions. *Optimal control of systems governed by partial differential equations.* Translated from the French by S. K. Mitter. Die Grundlehren der mathematischen Wissenschaften, Band 170. Springer-Verlag, New York, 1971.

[28] M.C. Mackey. Unified hypothesis for the origin of aplastic anemia and periodic hematopoiesis. *Blood*, 51(5):941–956, 1978.

[29] R. May. *Stability and Complexity in Model Ecosystems*. 1975.

[30] R. Palma-Behnke, C. Benavides, F. Lanas, B. Severino, L. Reyes, J. Llanos, and D. Sez. A microgrid energy management system based on the rolling horizon strategy. *IEEE Transactions on Smart Grid*, 4(2):996–1006, 2013.

[31] Huyên Pham. *Continuous-time stochastic control and optimization with financial applications*, volume 61. Springer Science & Business Media, 2009.

[32] E. M. Purcell. Life at low reynolds number. *American Journel of Physics*, 45:3–11, 1977.

[33] H.M. Robbins. Junction phenomena for optimal control with state-variable inequality constraints of third order. *J. of Optimization Theory and Applications*, 31:85–99, 1980.

[34] H. Seywald and E.M. Cliff. Goddard problem in presence of a dynamic pressure limit. *Journal of Guidance, Control, and Dynamics*, 16(4):776–781, 1993.

[35] Fredi Tröltzsch. *Optimal control of partial differential equations*, volume 112 of *Graduate Studies in Mathematics*. American Mathematical Society, Providence, RI, 2010. Theory, methods and applications, Translated from the 2005 German original by Jürgen Sprekels.